J. Fluid Mech. (1990), *vol.* 218, *pp.* 377–403
Printed in Great Britain

Turbulent structure in a channel flow with polymer injection at the wall

By D. T. WALKER[1] AND W. G. TIEDERMAN[2]

[1] Department of Naval Architecture and Marine Engineering, The University of Michigan, Ann Arbor, MI 48109-2145, USA

[2] School of Mechanical Engineering, Purdue University, West Lafayette, IN 47907, USA

(Received 10 May 1989 and in revised form 1 February 1990)

Two-component laser velocimeter measurements in a fully developed turbulent water channel flow with polymer injection were used to examine the effect of polymer injection on the Reynolds stresses and the production terms in the Reynolds stress transport equations. These measurements show that while the root-mean-square (r.m.s.) fluctuation level of the streamwise velocity was increased, the r.m.s. of the wall-normal velocity and the Reynolds shear stress were reduced. The decrease in the Reynolds shear stress resulted from altered contributions from the quadrants of the (u, v)-plane. Although the Reynolds shear stress decreased, the magnitude of the velocity fluctuation products which most contributed to that stress increased. Production of the streamwise Reynolds normal stress was decreased but production of the Reynolds shear stress was unchanged. This shows that the processes represented by pressure–strain correlation terms in the Reynolds stress transport equations may be directly affected by the polymer.

1. Introduction

Drag reduction resulting from the presence of long-chain, high-molecular-weight polymers in turbulent flow of liquids has received considerable attention since the initial publications of Toms (1949) and Mysels (1949). Although a thorough understanding of the way in which polymers reduce drag has proved elusive, the use of polymer drag reduction for engineering purposes has proceeded (see e.g. Hoyt 1984). The purpose of this study is to enhance our understanding by comparing the turbulent structure in a fully developed two-dimensional channel flow with that which occurs when a relatively small flow rate of drag-reducing polymer solution is injected through a wall slot into it. Previous investigations have examined the mean velocities and Reynolds stresses in flows with uniform polymer concentration. This study uses two-dimensional laser velocimeter measurements to examine these quantities along with the relevant production terms from the Reynolds stress transport equations as the flow evolves from the Newtonian state upstream of the wall-slot injector to a drag-reduced state downstream. Use of the Reynolds stress transport equations in interpreting these changes gives an indication of what aspects of the turbulence production and maintenance process are directly affected by the polymers.

Polymer solutions capable of causing drag reduction in turbulent flows are typically non-Newtonian, viscoelastic fluids. The polymer used in this study was an aqueous solution of SEPARAN AP-273, a polyacrylamide manufactured by Dow

Chemical. Argumedo, Tung & Chang (1978), Tsai & Darby (1978) and Cho, Hartnett & Park (1983), among others, have demonstrated that this polymer solution exhibits shear-thinning behaviour: the shear viscosity decreases with increasing shearing strain rate. Ryskin (1987) showed that, when drag-reducing polymer solutions are placed in a purely elongational strain, for example flow through an axisymmetric nozzle, the viscosity increased with increasing elongational strain rate. This 'extensional' viscosity can be up to two orders of magnitude larger than the shear viscosity. These results are evidence of the complex constitutive nature of polymer solutions.

Constitutive relations that model the steady and laminar shear response of the polymer solution have been proposed by Argumedo *et al.* and Tsai & Darby. Tsai & Darby also modelled the response of the fluid to certain transient inputs. At present these rheological models have not been implemented in numerical simulations of turbulent flow.

Near the polymer injector, the rheology of the water–polymer mixture is complicated by the presence of concentration variations. For the flow examined in this study, Walker & Tiederman (1989) showed that near the injector the instantaneous polymer concentration can vary from 0 to 500 p.p.m. in the near-wall region. Over this range of concentrations, the shear viscosity varies in a nonlinear way from values near the viscosity of water (about 1 cP) to more than 10 cP. It is clear that the other rheological properties also vary in some undetermined manner.

The average turbulent structure is described by the spatial variation of the terms in the Reynolds-averaged Navier–Stokes equations and the Reynolds stress transport equations. For an incompressible, stationary turbulent flow the Reynolds-averaged Navier–Stokes equations are

$$\rho \bar{U}_j \frac{\partial \bar{U}_i}{\partial x_j} = -\frac{\partial \bar{P}}{\partial x_i} + \frac{\partial}{\partial x_j}\left(\overline{\left(\mu \frac{\partial U_i}{\partial x_j} + \frac{\partial U_j}{\partial x_i}\right)} - \overline{u_i u_j}\right) + \ldots, \tag{1}$$

where $\bar{U}_i$ is the time-averaged mean velocity in the x_i direction and u_i is the fluctuation about that mean. Here, ρ is the fluid density, μ is the dynamic viscosity and $\bar{P}$ is the time-averaged mean pressure. This form of the equations allows for spatially varying viscosity. The non-Newtonian nature of the polymer solution requires additional terms which are not specifically specified here. The terms $\overline{u_i u_j}$ comprise the Reynolds stress tensor.

Transport equations for the elements of the Reynolds stress tensor for Newtonian fluids are given by (see e.g. Bradshaw 1978)

$$\begin{array}{cccc} & & \text{I} & \text{II} \\ \dfrac{\partial \overline{u_i u_j}}{\partial t} + \bar{U}_l \dfrac{\partial \overline{u_i u_j}}{\partial x_l} = & -\left(\overline{u_i u_l} \dfrac{\partial \bar{U}_j}{\partial x_l} + \overline{u_j u_l} \dfrac{\partial \bar{U}_i}{\partial x_l}\right) & + \overline{\dfrac{p'}{\rho}\left(\dfrac{\partial u_i}{\partial x_j} + \dfrac{\partial u_j}{\partial x_i}\right)} \\ & \text{III} & \text{IV} & \text{V} \qquad \text{VI} \\ & -\dfrac{\partial}{\partial x_l}\overline{(u_i u_j u_l)} - \dfrac{1}{\rho}\left(\dfrac{\partial}{\partial x_i}\overline{p' u_j} + \dfrac{\partial}{\partial x_j}\overline{(p' u_i)}\right) & + \nu \dfrac{\partial^2 \overline{u_i u_j}}{\partial x_l^2} - 2\nu \overline{\left(\dfrac{\partial u_i}{\partial x_l}\dfrac{\partial u_j}{\partial x_l}\right)} + \ldots. \end{array} \tag{2}$$

Here, p' is the instantaneous fluctuation about the mean pressure $\bar{P}$, and ν is the kinematic viscosity. The left-hand side of (2) represents the time rate of change and advection of a given Reynolds stress. Term I on the right-hand side of (2) represents production of Reynolds stress by interaction of the turbulent motion with the mean

rate-of-strain field. Term II accounts for the generation, destruction or redistribution between components by means of pressure fluctuations and is generally referred to as the pressure–strain correlation. The pressure–strain correlation causes the normal stresses to become more isotropic. Terms III and IV represent transport through turbulent fluctuations, with III accounting for transport by velocity fluctuations and IV for transport by pressure fluctuations. Viscous transport of Reynolds stress is represented by term V, and term VI represents generation or destruction due to viscous stress fluctuations. For flows with polymer injection additional terms would be required to account for spatially varying viscosity in the flow and the non-Newtonian behaviour of the fluid.

The spatial behaviour of the terms in (2) is presented by Mansour, Kim & Moin (1988) and Spalart (1988) for a fully developed channel flow and a zero-pressure-gradient boundary layer, respectively. These results were obtained by direct numerical simulation of turbulent flow of Newtonian fluids and show that, near the wall, the maintenance of turbulent stresses is dominated by production (I), dissipation (VI) and the effect of the pressure–strain correlations (II). Berman (1989) derived terms in the momentum and turbulence kinetic energy equations due to the interactions of turbulence with polymer molecules using a FENE dumbbell model. His results showed that for fully developed channel flow both the production and dissipation of turbulence kinetic energy were reduced relative to Newtonian flows.

The complete response of the turbulent structure to the introduction of a drag-reducing polymer solution can only be determined through experiment. Owing to the viscoelastic nature of drag-reducing polymers, measurements of velocity using hot-wire anemometers, hot-film devices or Pitot tubes can be in error (see Metzner & Astarita 1967). This leaves the laser velocimeter as the only viable method for measuring velocity and turbulence statistics in aqueous solutions. Most laser velocimeter investigations have been restricted to one-component velocity measurements although recently two-component velocity measurements have been made in flows with a uniform polymer concentration, by Willmarth, Wei & Lee (1987) and Luchik & Tiederman (1988).

The turbulence quantity most often measured is the profile of the mean streamwise velocity component, $\bar{U}$, reported by Berner & Scrivener (1980), McComb & Rabie (1982) and Bewersdorff (1984) for circular tubes, Rudd (1972) and Logan (1972) for square tubes, and Reischman & Tiederman (1975), Luchik & Tiederman (1988) and Willmarth *et al.* (1987) for rectangular channels. The effects of drag-reducing additives on the mean velocity profile (normalized with inner variables: $U^+ = \bar{U}/u_\tau$, $y^+ = yu_\tau/\nu$, where $u_\tau = (\tau_w/\rho)^{\frac{1}{2}}$, ν is the kinematic viscosity evaluated at the time-average wall strain rate and τ_w is the average wall shear) are clearly established. The linear sublayer ($y^+ < 8$) remains unaffected and the logarithmic overlap region is displaced toward higher velocities with a slope relatively unchanged from the Newtonian value.

The root mean square (r.m.s.) of the streamwise velocity (u') also exhibits specific trends in drag-reduced flows. In Newtonian flows the peak in u'/u_τ occurs at about $y^+ = 15$. For drag-reducing flows, this peak is shifted outward in both physical distance and y^+. The results presented by Luchik & Tiederman (1988) and Willmarth *et al.* (1987) show that the r.m.s. of the normal velocity, v', decreases both physically and nondimensionally throughout the viscous sublayer. Similar results were obtained by Logan (1972) but the interpretation of those results was complicated by the effect of secondary flows on the shear velocity in the square duct used in that study.

Luchik & Tiederman (1988) also measured the turbulent shear stress, $\overline{uv}$, and found that the location of the peak in $\overline{uv}$ moved outward and the peak value was decreased. Willmarth *et al.* (1987) found $\overline{uv}$ greatly decreased across the entire flow and proposed the existence of a non-Newtonian retarding force to account for the discrepancy between the total stress and the sum of the turbulent and mean viscous shear stresses. This behaviour was not seen in the experiments of Luchik & Tiederman, where the polymer was mixed uniformly with the flow, but is similar to that presented by Bewersdorff (1984) for pipe flows where a very high-concentration polymer solution was injected at the centreline.

These studies indicate that the presence of polymers in a turbulent flow results in significant changes in the Reynolds stresses. The behaviour of the terms in the Reynolds stress transport equations has not been examined for these flows and the mechanism(s) by which the polymer solutions cause these structural changes have not been identified.

In a flow with polymer injection, the turbulent structure evolves from a fully developed, Newtonian flow to a flow in a drag-reduced state. This evolution is the result of direct modification of the terms in the momentum equation and the Reynolds stress transport equations due to the presence of the polymer solution. The present study focuses upon important terms in these equations which are present in both Newtonian and non-Newtonian flows. In the momentum equation, these terms include the Reynolds stresses. In the Reynolds stress transport equation, the production terms (I in equation (2)), the pressure–strain correlations (II) and the viscous dissipation terms (VI) also occur in both types of flow. These quantities represent most of the important processes in the near-wall region for Newtonian flows and their significance is expected to be undiminished in flows of polymer solutions. In this study the Reynolds stresses and production terms are measured directly using a two-component laser velocimeter. By examining the response of these measured quantities to the presence of the polymer solution, the behaviour of the other significant terms which cannot be measured (i.e. the pressure–strain correlation and the viscous dissipation terms) may be inferred. In this way, the effects of the polymer on the processes responsible for the maintenance of turbulent stresses in wall flows are identified. The modification by the polymer solution of velocity fluctuations contributing to the Reynolds shear stress $\overline{uv}$ is also examined in detail. These effects result in changes in the Reynolds stresses which in turn are responsible for the macroscopic phenomenon of drag reduction.

In the next section, the experimental facilities and the apparatus and procedures used for this investigation are discussed. Measurements of turbulence structure for the fully developed channel flow (no injection) are presented to establish the 'standard' character of the basic water flow. These data serve as a measure by which modification to the flow can be detected and demonstrate the accuracy of the data. The latter is very important, since the mean velocity gradient must be estimated to evaluate the production term in equation (2). Also, a highly accurate method for determining the wall shear stress in fully developed flows is shown. The concentration field in injected flows is then discussed briefly. Changes in the mean quantities and Reynolds stresses resulting from the developing concentration field are discussed, and the causes of these changes are inferred from examination of the Reynolds stress transport equations. The detailed behaviour of the velocity fluctuations is then examined. In these results, the effect of the injection process on fluctuation structure is isolated from the modification of the flow by the polymers by examining a flow with water injection.

2. Apparatus and procedure

2.1. *Experimental facilities*

The water flow loop used in these experiments, shown in figure 1, was driven by four ninety gallon per minute centrifugal pumps operating in parallel. At each end of the test section there was a large stilling tank to isolate the test section from any hydrodynamic disturbances in the flow loop. The upstream stilling tank contained a perforated plate followed by a screen and open-cell sponge section, and a smooth two-dimensional contraction at the outlet. The inlet of the channel was preceded by a flow straightener consisting of closely packed plastic drinking straws which ensured that no large-scale vorticity existed in the channel entry flow. The downstream tank contained a perforated plate to damp out disturbances and a copper coil through which cooling water was passed to maintain the channel water at a constant temperature.

The flow loop had a rectangular-cross-section channel (6.0 cm high by 57.5 cm wide) as the test section. The test section was constructed from $\frac{1}{2}$ in. acrylic and polycarbonate sheet and was more than 100 channel heights long. Polymer solutions were injected through flush-mounted, angled slots located in both of the 57.5 cm walls of the channel. The injection slots had a width, measured in the streamwise direction, of 2.5 mm and were inclined 25° to the flow direction as shown in figure 2. The injectors were located about 80 channel heights downstream of the inlet.

The coordinate system used in the description of the apparatus and presentation of the results is also shown in figure 2. The x-axis is parallel to the flow direction and the y-axis is normal to the flow direction and the long (57.5 cm) dimension of the channel cross-section. The origin of this coordinate system is located at the centre (mid-span) of the injection slot in the lower 57.5 cm wall of the channel.

2.2. *Polymer solution preparation*

The additive was an aqueous solution of SEPARAN AP-273, a polyacrylamide manufactured by Dow Chemical, at a concentration of 700 p.p.m. based on weight. The dry powder was suspended in 300 ml of isopropyl alcohol and mixed into filtered, deaerated tap water at about 38 °C using a magnetic stirrer. The concentration of this initial mixture was about 5000 p.p.m. and it was allowed to hydrate for 12 to 24 hours. This solution was then diluted to 700 p.p.m. using filtered tap water and allowed to hydrate for 12 to 24 hours before using.

The repeatability of the polymer solutions was confirmed in two ways. The steady shear viscosity was checked over a range of shear rates using a Brookfield LVT-SCP3 cone and plate viscometer. Also, samples of each batch were diluted to 100 p.p.m. and drag reduction was measured in a 1.405 cm diameter tube for a range of flow rates. Only polymer solutions which yielded consistent results in these two measures were used.

2.3. *Two-component laser velocimeter system*

The laser-velocimeter transmitting optics consisted of a Thermo-Systems Incorporated (TSI) model 9100-8 system incorporating a Lexel model 85.5 500 mW argon-ion laser. This is a two-component, three-beam system where velocities are measured using one blue (488 nm) beam, one green (514.5 nm) beam, and a blue–green beam containing both wavelengths. Both channels were frequency shifted 40 MHz using a single Bragg cell ahead of the colour separator. The beam spacing was 25 mm and the beams were expanded to 2.5 mm and focused with a 250 mm transmitting lens.

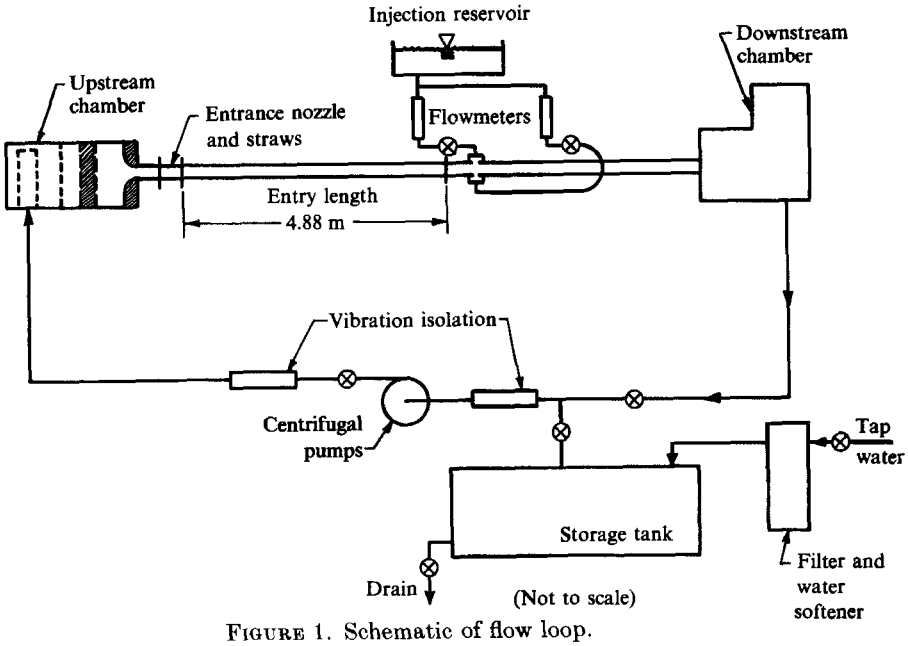

FIGURE 1. Schematic of flow loop.

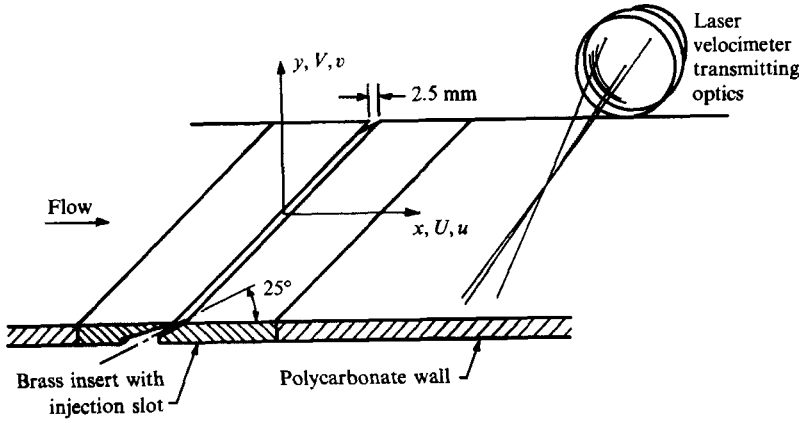

FIGURE 2. Injection slot and coordinate system.

Modifications to the standard TSI 9100-8 system consisted of the following. The beam displacer in the output end of the model 9112-1 dichroic colour separator was rotated 90° to place the green beam at 90° from the blue beam. After the colour separator, the blue–green beam was displaced to the optical axis using a TSI 9174 50 mm beam displacer. These changes placed the blue–green beam on the optical axis and the blue beam and green beam at nominally $\pm 45°$ from vertical. In this way, velocity components at $\pm 45°$ to the flow direction were measured.

The test section was viewed through plate glass windows located in the 6.0 cm channel endwalls. These windows were flat within ± 3 μm and minimized beam deflection by the channel walls. This ensured that optimum signal quality was obtained and that accurate measurements of spatial location were possible. The location of the measurement volume relative to the wall was determined using a TSI model 9140 receiving optics assembly and eyepiece installed in the transmitting

optics. By moving the probe volume toward the wall, the y-location where the image of the probe volume intersected the wall could be determined to within about one-half the probe volume diameter. This position was then used as a reference for all subsequent vertical location measurements.

The receiving optics were standard TSI two-component items. Scattered light was collected in forward scatter using a 250 mm focal length lens. A 2.27X telescope was inserted behind the collection lens to increase the spatial resolution of the receiving optics. A 50 μm aperture was used in a TSI 9143 field-stop assembly to ensure spatial coincidence of the two measured velocities. The light passing through the aperture was recollimated and passed through a dichroic colour separator. The separate colours were bandpass filtered and focused on two photomultiplier tubes.

The spatial resolution of the measurement system is defined by both the configuration of the transmitting optics and the receiving optics. The axis of the receiving optics was located in the (y, z)-plane at an angle of 9.5° from the axis of the transmitting optics. For this orientation, the extent of the probe volume in the y-direction is defined by the diameter of the beam intersection ($l_y = 63$ μm). The x-dimension of the measurement volume is determined by the diameter of the field of view of the receiving optics ($l_x = 55$ μm). The length of the probe volume along the z-axis defined by the field of view of the receiving optics and the collection angle, was $l_z = 330$ μm. Non-dimensionalizing with the shear velocity and kinematic viscosity of the water flow yields: $l_x^+ = 1.6$, $l_y^+ = 1.8$, and $l_z^+ = 9.6$.

The photomultiplier output for each channel was high-pass filtered at 25 MHz to remove the pedestal frequencies and was electronically down-mixed to yield an effective shift frequency of 0.5 MHz using a TSI model 9186 down-mixer. The frequency of the down-mixed signals was determined using two TSI 1980 counter processors. These data were acquired using a Masscomp 5520 microcomputer communicating with the TSI model 1998 interface through a Masscomp PI16F fast parallel interface. Data were not transferred to the computer unless measurements were made on both channels within a predetermined coincidence window. The length of the coincidence window was set equal to the estimated minimum transit time through the probe volume (about 100 μs).

2.4. *Seeding, sampling and velocity bias*

The major problem with laser velocimetry is that the fluid velocity must be deduced by measuring the velocity of particles suspended in the fluid. To obtain accurate fluid velocities no more than one particle can be in the measurement volume at any given time. The estimated velocity statistics must also be unaffected by fringe bias, filter bias, or velocity bias (see Edwards 1987).

For this study the flow was seeded with homogenized whole milk which contains fat particles about 0.3 μm in diameter. To ensure that the flow was uniformly seeded, the injected fluids were seeded at the same concentration as the water in the flow loop. In the case of the polymer solutions, this was accomplished by adding the seed to the water used to dilute the solution to its final concentration.

The maximum particle arrival rate achievable with only one particle in the measurement volume on average can be estimated by dividing the velocity of the flow by the diameter of the probe volume. For the flow in question this results in a particle arrival rate of about 4 kHz to 8 kHz, depending on position in the flow. For the results presented here, the water in the flow loop was prepared by filtering with a diatomaceous earth filter to remove the natural hydrosol present in the water. The water was then seeded at a concentration of 15 ml/1000 l which resulted in

maximum validation rates of about 2 kHz. This ensured that the probability of having more than one particle in the probe volume at any given time was minimized.

Fringe bias was overcome by frequency shifting. The effective fringe velocity (after down-mixing) was more than three times the maximum velocity in the flow. This provided almost uniform angular response for the velocity measurements. The possibility of filter bias was eliminated by setting the filters in the signal processors to yield a pass-band equivalent to ± 2.5 m/s which is ± 3 times the centreline velocity, U_0.

Velocity bias occurs because there is a higher probability of measuring a high-velocity particle than a low-velocity particle (see McLaughlin & Tiederman 1973). For the flow in question, which has a turbulence intensity of 30–40% near the wall, the error in the estimate of the mean velocity would be as large as 15% if this effect was ignored. For the two-component measurements, velocity bias was eliminated using the fixed-waiting-time sampling method. In this method the data acquisition system is inhibited for a fixed amount of time between one realization and the next. The validation rate was maintained at about five times the Kolmogorov frequency and the inhibit time was ten times the inverse of the validation rate. (The Kolmogorov timescale was estimated by assuming that dissipation of turbulence kinetic energy was equal to production at the production peak). Based on the results of Gould, Stevenson & Thompson (1989), this approach should be adequate to eliminate velocity bias effects from the mean quantities and it is assumed that the effects on higher statistical moments are also eliminated.

Large data sets were used to reduce, as much as was practical, the error inherent in estimating statistics from finite-size ensembles. For the water flow results, all statistics were based on ensembles of 25000 independent realizations for each velocity component. Statistics for the flows with water and polymer injection were calculated using ensembles of 10000 independent realizations. This resulted in an uncertainty of less than 0.5% on $\bar{U}$, 1% on u', 2% on v' and up to 7% on $\overline{uv}$ at 95% confidence. Except for very near the wall, this was the dominant source of error in the calculated statistics; for $y^+ \lesssim 10$ the uncertainties are larger owing to decreased signal quality.

3. Results

3.1. *Water flow*

Measurements in the water flow with no injection were made 100 mm downstream of the injector. This type of channel flow has been studied by many investigators. Hussain & Reynolds (1975) performed one-component hot-wire velocity measurements in an air flow in a 32:1 aspect-ratio channel which minimized endwall effects. Kreplin & Eckelmann (1979) examined the near-wall structure of an oil channel flow where, owing to the high viscosity, excellent spatial resolution was obtained with hot-film probes. Wei & Willmarth (1989), made high-spatial-resolution, two-component laser velocimeter measurements over a range of Reynolds numbers. Kim, Moin & Moser (1987) and Mansour *et al.* (1988) have also presented results from a full numerical simulation of turbulent channel flow.

Integral parameters for the water flow are presented in table 1 along with the values of the major flow variables. Integration of the mean velocity profile yielded a mass-averaged velocity, U_m, of 0.574 m/s. The Reynolds number based on mass-averaged velocity and channel height was 36000 and the momentum-thickness Reynolds number was 1770.

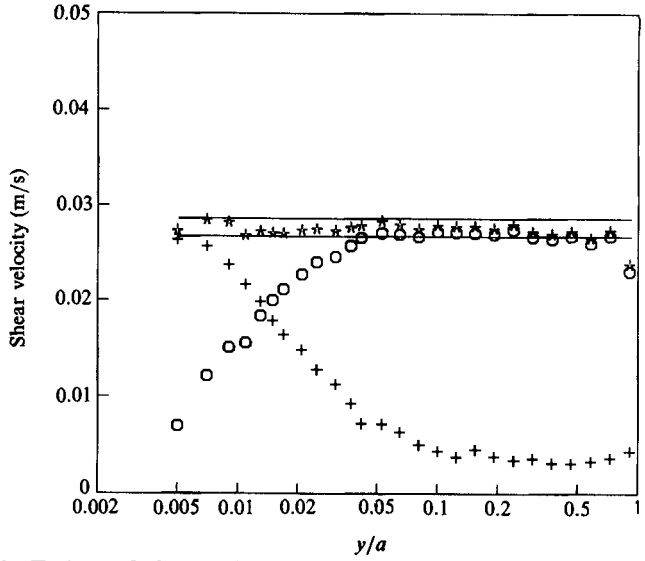

FIGURE 3. Estimated shear velocity for water flow with no injection: *, u_τ: +, viscous contribution; O, turbulent contribution; =, 95% confidence interval.

$U_m = 0.574$ m/s	$h = 60.0 \times 10^{-3}$ m
$U_0 = 0.651$ m/s	$\nu = 0.957 \times 10^{-6}$ m^2/s
$u_\tau = 27.6 \times 10^{-3}$ m/s	$Re_h = \dfrac{U_m h}{\nu} = 36000$
$\delta^* = 3.45 \times 10^{-3}$ m	$Re_\delta = \dfrac{U_0 h}{2\nu} = 20400$
$\theta = 2.61 \times 10^{-3}$ m	$Re_\theta = \dfrac{U_0 \theta}{\nu} = 1770$

TABLE 1. Experimental conditions for water flow with no injection

The shear velocity, u_τ, for the water flow with no injection was determined using the linear variation of total shear stress for a fully developed flow:

$$\tau_{\text{total}} = \mu \frac{d\bar{U}}{dy} - \rho \overline{uv} = \tau_w (1 - y/a), \tag{3}$$

where a is the channel half-height. Rearranging and using the definition of shear velocity, $u_\tau = (\tau_w/\rho)^{\frac{1}{2}}$ results in

$$u_\tau = u_\tau(y) = \left[\frac{\nu \, d\bar{U}/dy - \overline{uv}}{(1 - y/a)} \right]^{\frac{1}{2}}. \tag{4}$$

An estimate of the shear velocity at each y-location is determined from (4) using the measured value of $\overline{uv}$ and the estimated value of the mean velocity gradient for each measurement location. The values for all y-locations are then averaged to determine the shear velocity for the flow. Figure 3 illustrates the implementation of this technique. The value of the shear velocity was 0.0276 ± 0.0010 m/s at 95%

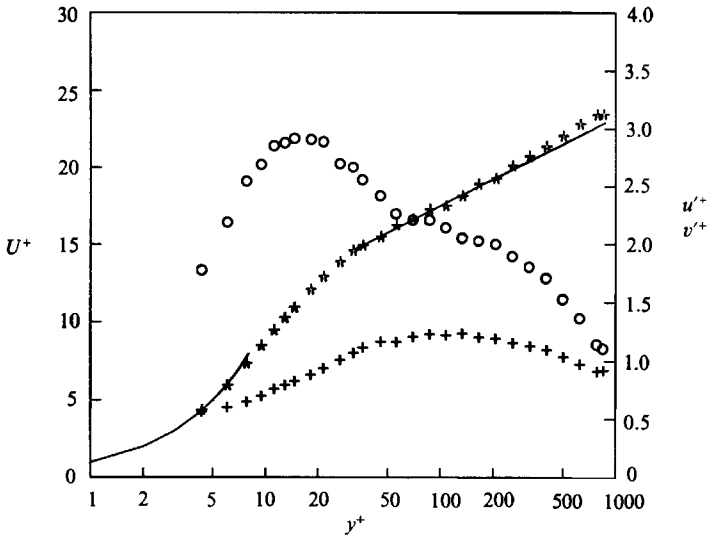

FIGURE 4. Turbulence statistics for fully developed channel flow: *, $\bar{U}/u_\tau$; ○; u'/u_τ; +, v'/u_τ.

confidence. This is equivalent to a strain rate of 798 s^{-1} at the wall, a viscous length ν/u_τ of 0.0346 mm and $y^+ = 867$ at the channel centreline.

Since the flow is fully developed, static pressure drop should be proportional to the wall shear stress (if one assumes that this high-aspect ratio channel approximates flow between infinite parallel plates). The value of shear velocity calculated from the static pressure drop is about 10% higher than the value determined from the total shear stress. This is due to the presence of secondary flows in the corners and the larger wetted area of the 10:1 aspect-ratio channel.

Figure 4 shows the mean streamwise velocity profile normalized with shear velocity and kinematic viscosity. The two solid lines in the figure represent the near-wall variation in U^+,

$$U^+ = y^+, \tag{5}$$

and the relationship for the logarithmic overlap region

$$U^+ = \frac{1}{\kappa}\ln y^+ + B. \tag{6}$$

There is good agreement between the line and the data in the linear region and there is good correspondence with the logarithmic law using $\kappa = 0.41$ and $B = 6.0$ (Luchik & Tiederman 1987).

Figure 4 also shows the root-mean-square (r.m.s.) velocity fluctuation level for the streamwise and normal velocity components as a function of distance from the wall. These results have a maximum u'^+ of 2.9 at about $y^+ = 15$ and a u'^+ of about one at the channel centreline. The r.m.s. of the dimensionless normal velocity has a broad peak of about 1.2 centred near $y^+ = 100$, and v'^+ decreases to slightly less than one at the channel centreline. In general, these values for u'^+ and v'^+ agree well with Kreplin & Eckelmann (1979), and are slightly higher than the smallest sensor results of Ligrani & Bradshaw (1987). However, they are about 10% higher than those reported by Wei & Willmarth (1989), Hussain & Reynolds (1975) and Kim *et al.* (1987). Very near the wall ($y^+ \leqslant 10$) v'^+ appears to approach a constant value of 0.5. This disagrees with the results of Kim *et al.* (1987) and Finnicum & Hanratty (1985)

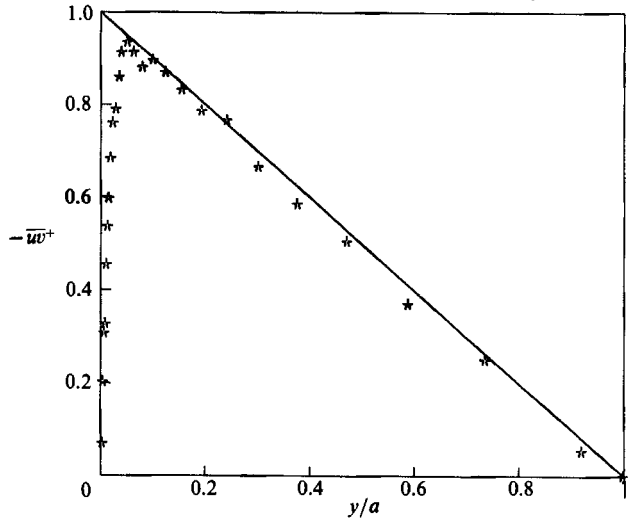

FIGURE 5. Turbulent shear stress for fully developed channel flow; ——, total shear stress (equation (4)).

which both reported that $v' \sim y^2$ near the wall. This indicates that the measurements of v' are in error for $y^+ \leqslant 10$. These errors result from two contributing factors: the inevitable decrease in signal quality for laser velocimeter measurements as one approaches a wall and the $\pm 45°$ orientation of the measured velocity components. The latter requires that v', which is small, be calculated from the difference between two nearly equal, larger magnitude quantities. The former increases the uncertainty in the measured quantities used to calculate v'. These two effects combine to affect the accuracy of the calculated v' values.

The effect of gradient broadening on the measured u' levels due to the finite size of the measuring volume is estimated to introduce about 6% error at $y^+ = 5$ and less than 1% error for $y^+ > 10$ (see Karpuk & Tiederman 1976). The results of Luchik & Tiederman (1986) show that for laser velocimeter measurements the r.m.s. levels are not affected by spatial averaging over the spanwise length of the probe as is the case with hot-wire and hot-film devices. Therefore, since the uncertainty in u_τ is small, these results are believed to accurately represent the turbulence structure.

The turbulent shear stress $\overline{uv}$ is shown in figure 5 normalized with u_τ; also shown is a line representing the linear variation in total shear across the channel. Away from the wall, where the mean viscous shear is small, the agreement between the line and the data is excellent.

Equation (3) can be solved for $\overline{uv}$:

$$-\overline{uv} = \frac{1}{\rho}\left[\tau_w\left(1-\frac{y}{a}\right)-\mu\,\mathrm{d}\bar{U}/\mathrm{d}y\right]. \tag{7}$$

Figure 6 shows the same data on a semi-log coordinates, which allows a more detailed examination of the near-wall region, along with a line representing (7) (the values determined from subtracting the mean viscous shear stress from the total shear stress). There is good agreement between these two values, although there is some scatter in the data near the peak in $-\overline{uv}$.

The correlation coefficient $R_{uv} = -\overline{uv}/u'v'$ is a measure of how strongly the u- and v-fluctuations are correlated, i.e. the degree to which the velocity fluctuations

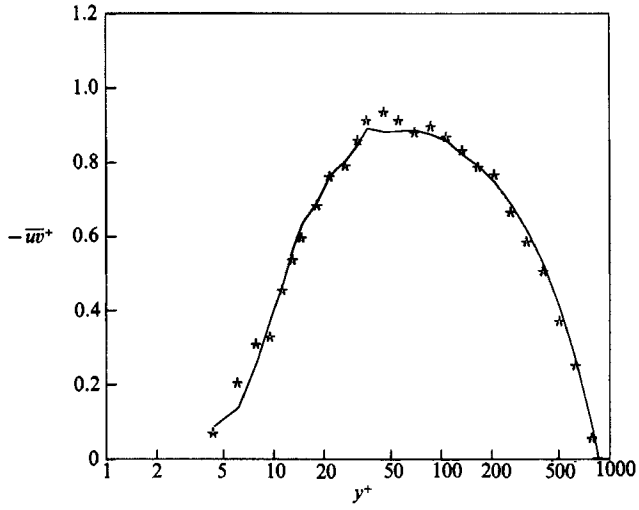

FIGURE 6. Turbulent shear stress for fully developed channel flow; ——, equation (7).

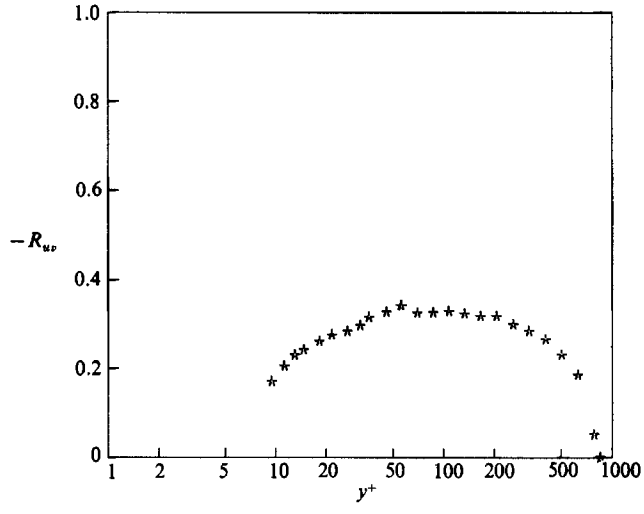

FIGURE 7. Correlation coefficient for fully developed channel flow.

contribute to momentum transport. The peak value of R_{uv}, shown in figure 7 is about 0.35 which is lower than the value in the numerical simulations of Moin & Kim (1982) (~ 0.4 at $Re = 24300$) and Kim *et al.* (1987) (0.45–0.50 at $Re = 5600$). The results of Wei & Willmarth (1989) decrease from 0.45 to 0.35 as Reynolds number increases from 30000 to 80000. Assuming the trend toward lower peak values with increasing Reynolds number is correct, the present results are compatible with the numerical results, although they are somewhat higher than those of Wei & Willmarth. The occurrence of a local peak in R_{uv} near $y^+ = 12$ which occurs in the channel flow computations of Moin & Kim (1982), Kim *et al.* (1987) and Moser & Moin (1987) does not agree with the present experimental results.

Figure 8 shows the $\overline{u^2}$ production profile normalized with shear velocity and kinematic viscosity. Also shown is a line representing this quantity calculated using the value of $\overline{uv}$ from (7). The agreement between the two results is excellent and they compare favourably with results presented by Mansour *et al.* (1988), Spalart (1988)

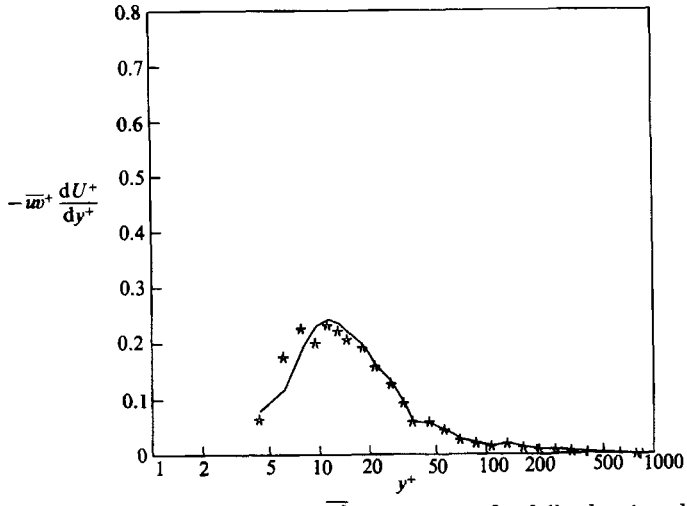

FIGURE 8. Reynolds stress production ($\overline{u^2}$ component) for fully developed channel flow; ——, production calculated using $-\overline{uv}$ from equation (7).

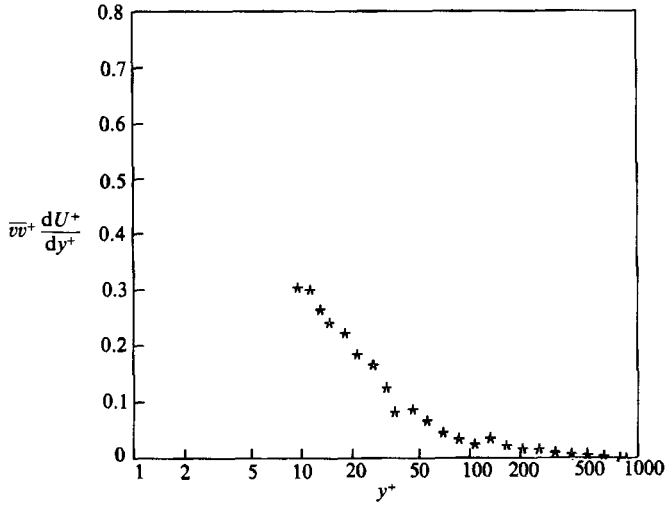

FIGURE 9. Reynolds stress production ($\overline{vv}$ component) for fully developed channel flow.

and Nagano & Hishida (1985). Reynolds shear stress ($\overline{vv}$) production is shown in figure 9. This quantity has a peak near $y^+ = 10$ that is significantly higher than that reported by Spalart (1988), Mansour *et al.* (1988) and Nagano & Hishida (1985). Those studies all showed a peak of about 0.1–0.15 at $y^+ = 15$–20.

3.2. *The structure of turbulence in injected flows*

To examine the effect of the evolving polymer concentration field on the structure of turbulence, two-component velocity measurements were made while injecting a 700 p.p.m. aqueous solution of SEPARAN AP-273. The flow in the channel was maintained at the conditions for the flow with no injection. Injection occurred at both the top and bottom walls at a flow rate equal to the mass flow rate through the linear portion of the viscous sublayer of the undisturbed channel flow. The polymer concentration and injection flow rate were those determined to be optimum for

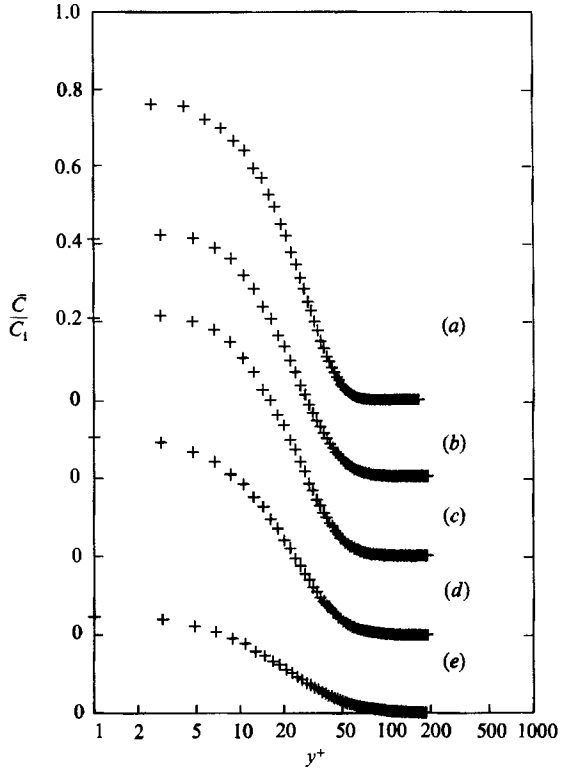

FIGURE 10. Mean concentration profiles for injected flows: (*a*) x = 10 mm, (*b*) 25 mm, (*c*) 50 mm, (*d*) 100 mm, (*e*) 200 mm.

producing drag reduction by Walker, Tiederman & Luchik (1986). This injection resulted in 25% drag reduction in the region from 50 to 150 mm downstream of the injector and a peak drag-reduction level of 44% in the region from 150 to 250 mm based on the measured change in the static pressure drop. Measurements of turbulent structure were made at locations 25, 50, 100 and 200 mm downstream of the injector (x^+ = 730, 1450, 2910 and 5810 respectively). To determine the effect of injection alone, two-component velocity measurements were made at x = 25 mm in a flow with water injection at the same mass flow rate.

Unless otherwise indicated, the results are normalized with the shear velocity for the fully developed flow without injection. The distance from the wall is normalized with this shear velocity and the kinematic viscosity of the channel water. These normalizations are for reference only and are not meant to imply any scaling arguments. Included, also for reference, are lines representing the appropriate results from the fully developed flow.

Figure 10 shows mean polymer concentration profiles as a function of distance downstream of the injector. These results were acquired using a laser-induced fluorescence technique (see Walker & Tiederman 1989). The near-wall mean concentration is 0.75 at x = 10 mm and then levels off at about 0.62 from 25 to 50 mm downstream of the injector. At x = 100 mm the near-wall concentration is reduced to 0.5 and at 200 mm it is down to 0.25. For $x \leqslant 100$ mm the thickness of the high-concentration layer at the wall is about 75 wall units and only at x = 200 mm does it extend beyond y^+ = 100. Other features of the concentration field for this flow are discussed by Walker & Tiederman (1989).

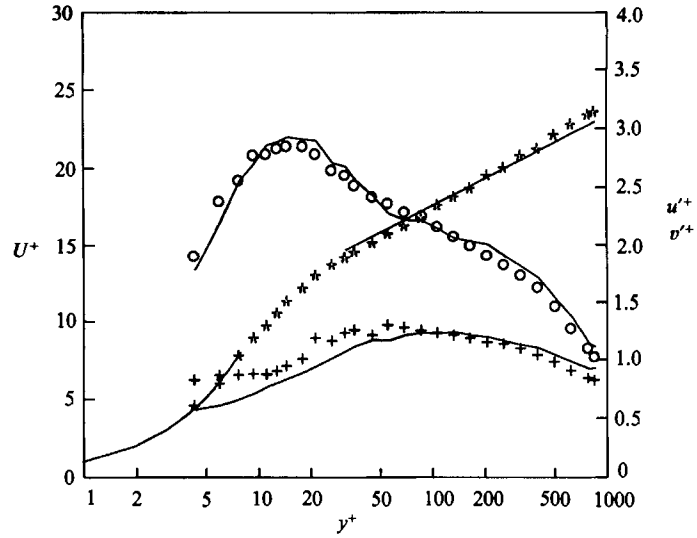

FIGURE 11. Turbulence statistics at $x = 25$ mm for flow with water injection: *, $\bar{u}/u_\tau$; ○, u'/u_τ; +, v'/u_τ; ——, fully developed flow.

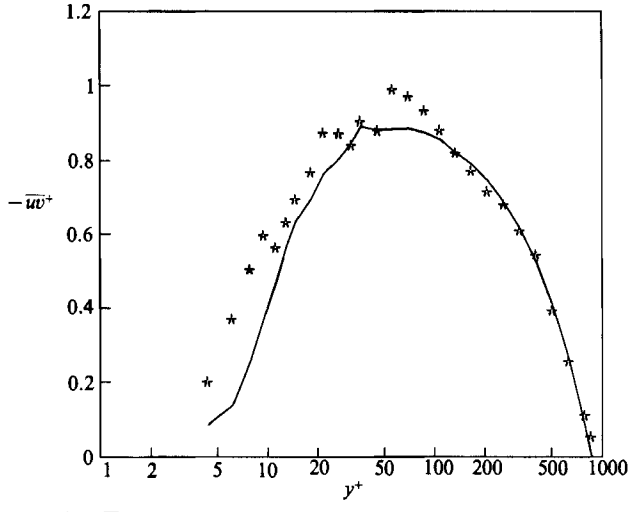

FIGURE 12. Turbulent shear stress profile for flow with water injection; ——, fully developed flow.

The mean velocity profile for the flow with water injection is compared to the standard channel flow profile in figure 11. There is a slight acceleration near the wall, and a slight deceleration for y^+ from 30 to about 100. For $y^+ > 200$ the injection has negligible effect. The region where the flow is modified corresponds roughly to the portion of the flow where the mean concentration is non-zero. Root-mean-square velocity fluctuations normalized with the shear velocity for the flow with no injection are also shown in figure 11. It is clear that while u' is virtually unchanged from the standard channel flow, the r.m.s. of the normal velocity is increased for $y^+ < 80$. The turbulent shear stress for the water injection flow is shown in figure 12. Compared to the standard channel flow, there is a general increase in $-\overline{uv}$ in the near-wall region. These results show that the major effects of the injection process on the structure of

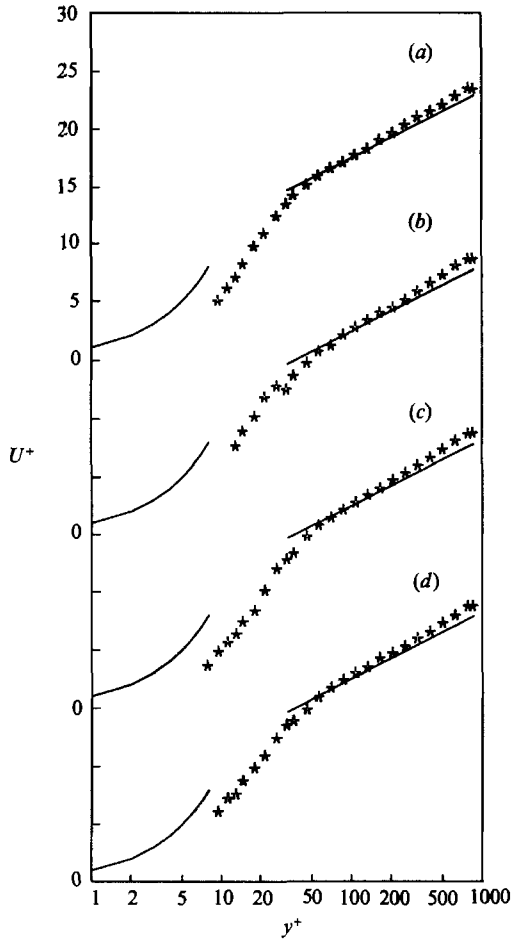

FIGURE 13. Mean velocity profiles for flow with polymer injection: (*a*) $x = 25$ mm, (*b*) 50 mm, (*c*) 100 mm, (*d*) 200 mm; ——, fully developed flow.

turbulence are to increase the turbulent shear stress and the r.m.s. of the normal velocity in the near-wall region where the injected fluid is concentrated.

Figure 13 shows the mean velocity profiles for x-locations between 25 and 200 mm downstream of the injectors during polymer injection. The outer flow ($y^+ \geqslant 50$) has accelerated slightly for all streamwise locations while near the wall the flow has decelerated. This is the opposite of what occurred for water injection. The region of deceleration corresponds to the high-concentration wall layer, indicating that the deceleration is related to the presence of the polymer solution (due to both an increase in viscosity and the onset of drag reduction). The reduction in velocity near the wall, which is responsible for the acceleration of the outer flow, is relatively constant for the first three streamwise locations and is slightly smaller at the 200 mm station.

For polymer injection, the r.m.s. fluctuation levels for the streamwise velocity are shown in figure 14. There is a 15% increase in peak fluctuation level at all x-locations and the peak has moved outward from $y^+ = 15$ to about 30. Near the wall, the r.m.s. level has decreased, while in the region where the polymer concentration is small ($y^+ \geqslant 50$) there is no change relative to the water flow. Figure 15 shows the r.m.s. fluctuation level of the normal velocity. At $x = 25$ mm the r.m.s. level is increased

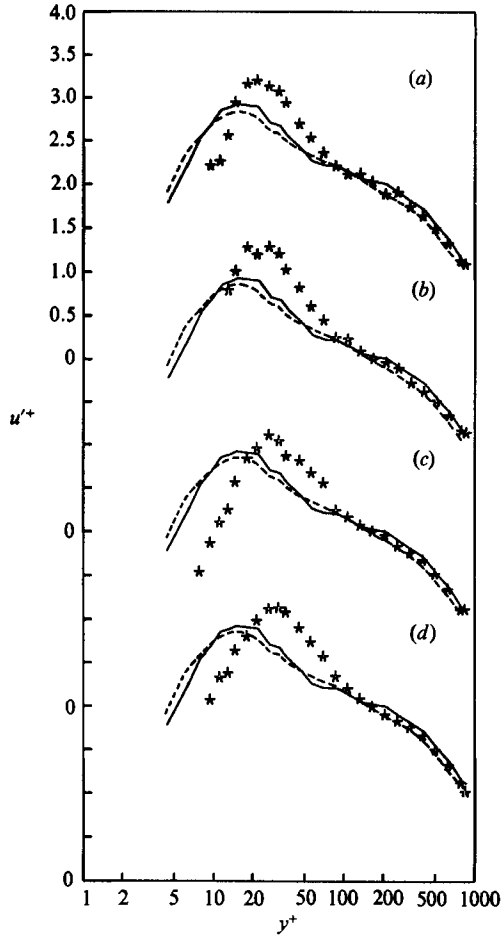

FIGURE 14. Root-mean-square velocity fluctuation (u'/u_τ) profiles for flow with polymer injection: (*a*) $x = 25$ mm, (*b*) 50 mm, (*c*) 100 mm, (*d*) 200 mm; ——, fully developed flow; – – – –, flow with water injection.

near the wall, similar to the behaviour in the flow with water injection. Near the wall, v' decreases with streamwise distance. The damping of v' extends significantly beyond the high-concentration wall layer (based on the mean concentration profile) for $x = 100$ mm and 200 mm. Similar behaviour was seen by Walker & Tiederman (1987). This previous study, which examined only mean concentration profiles, did not show, however, that the polymer solution instantaneously extends beyond $y^+ = 150$ yielding non-zero r.m.s. concentration levels in this region (see Walker & Tiederman 1989).

Reynolds shear stress profiles for polymer injection are shown in figure 16. At $x = 25$ mm the maximum in $-\overline{uv}$ is about 15% higher than the water flow. This level is significantly higher than for the flow with water injection indicating that the injection of the polymer solution causes more disturbance to the flow than water injection. Elevated $-\overline{uv}$ levels persist to the next streamwise station, $x = 50$ mm. At $x = 100$ mm the levels of $-\overline{uv}$ are significantly reduced over the entire near-wall region. This reduction is increased at $x = 200$ mm so that for $y^+ < 30$, $-\overline{uv}$ is near zero and the peak $-\overline{uv}$ is reduced by more than 25% and is moved away from the wall to about $y^+ = 200$. In a manner similar to that for v', $\overline{uv}$ is reduced in the near-

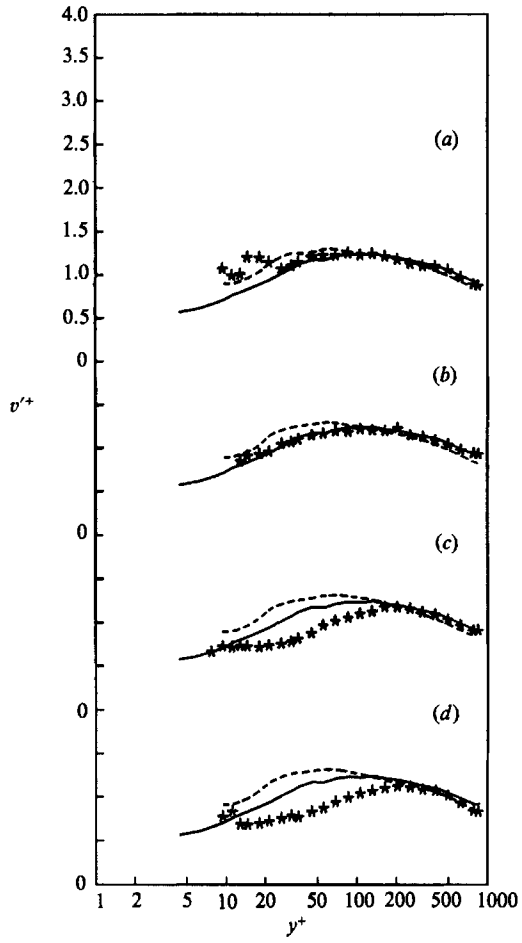

FIGURE 15. Root-mean-square velocity fluctuation (v'/u_τ) profiles for flow with polymer injection: (*a*) $x = 25$ mm, (*b*) 50 mm, (*c*) 100 mm, (*d*) 200 mm; ——, fully developed flow; – – – –, flow with water injection.

wall region and this effect extends beyond the high-concentration layer at the two downstream locations.

The correlation coefficient R_{uv} is shown in figure 17. At $x = 100$ mm and 200 mm, R_{uv} is significantly decreased in the near-wall region. This means that the decreased $-\overline{uv}$ levels that occur at these streamwise locations are not a result of a general decrease in the fluctuation level, but result from a smaller contribution from the fluctuations to net momentum transport. A closer look at this decrease will come later when the joint probability density function of uv is discussed.

Figures 18 and 19 show the production terms which appear in the Reynolds stress transport equations. For the normal stress $\overline{u^2}$, shown in figure 18, production (term I in equation (2)) is increased at $x = 25$ mm and 50 mm owing to the increase in $\overline{uv}$ which is the result of the injection process. At $x = 100$ mm the production has significantly decreased in the high-mean-concentration wall region, and at $x =$ 200 mm production has been virtually eliminated. Shear stress production, shown in figure 19, shows a marked increase at the two upstream locations due to the increase in v' resulting from the injection process. At the two downstream locations, production is essentially the same as in the water flow.

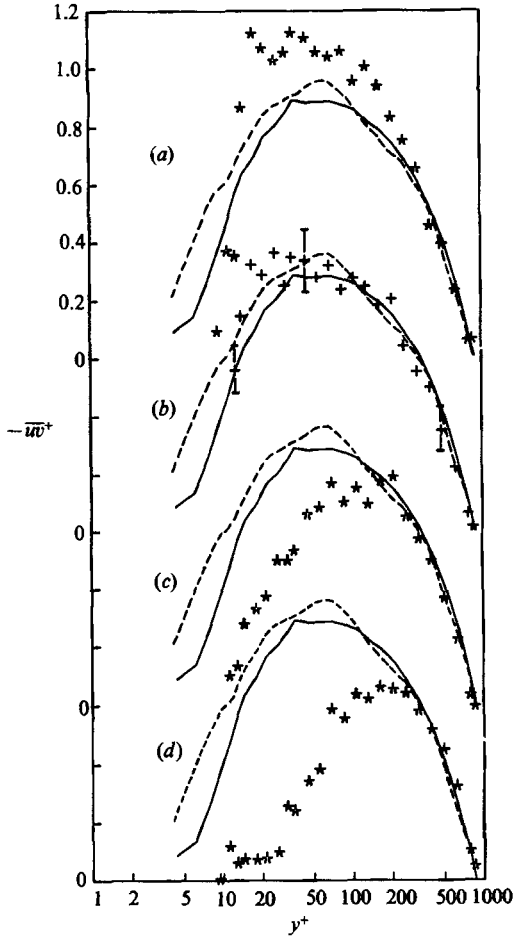

FIGURE 16. Turbulent shear stress profiles for flow with polymer injection: (*a*) $x = 25$ mm, (*b*) 50 mm, (*c*) 100 mm, (*d*) 200 mm; ——, fully developed flow; – – – –, flow with water injection.

These results are surprising considering the behaviour of the Reynolds stresses themselves. Although normal-stress production is virtually eliminated by $x = 200$ mm, u' remains elevated and essentially constant with respect to distance from the injector; meanwhile, v' decreases with streamwise distance. An increase or decrease in the rate of the destruction due to viscous stress fluctuations (term VI in (2)) would affect all stresses more or less equally since over the range of lengthscales which contribute to term VI the turbulence is nearly isotropic. Energy is produced in the $\overline{u^2}$ component of the Reynolds stress tensor and then transferred to the other components. The behaviour of u' and v' indicates that this transfer is inhibited. This may result from unknown viscous effects which arise from the non-Newtonian character of the polymer solutions. However, for Newtonian flows energy is transferred from $\overline{u^2}$ to $\overline{v^2}$ through the pressure–strain correlations (term II). The observed behaviour of the normal Reynolds stresses indicates that the processes represented by the pressure–strain correlations may be altered by the presence of the polymer solution.

The turbulent shear stress was observed to decrease significantly with streamwise position while the production rate for this stress was essentially unchanged from that of the water flow. Spalart (1988) and Mansour *et al.* (1988) showed that viscous stress

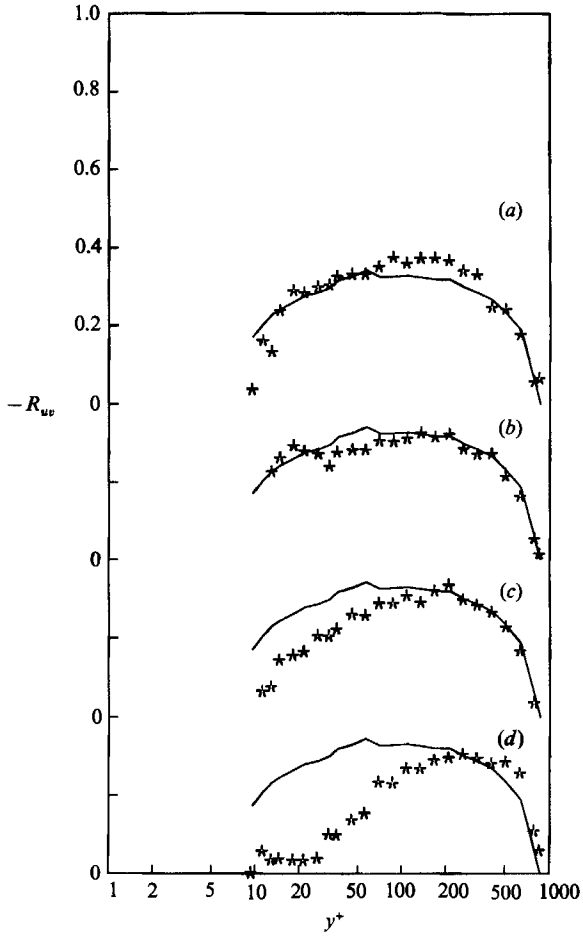

FIGURE 17. Correlation coefficient for flow with polymer injection: (*a*) $x = 25$ mm, (*b*) 50 mm, (*c*) 100 mm, (*d*) 200 mm; ——, fully developed flow.

fluctuations play only a minor role in the destruction of the turbulent shear stress; the dominant destruction mechanism is represented by the pressure–strain correlation (term II). This indicates that the mechanism which apparently modifies the pressure–strain correlations and inhibits the transfer of energy between the normal stresses may also cause increased destruction of the Reynolds shear stress.

These results have all been scaled with the shear velocity and kinematic viscosity of the water flow with no injection. This was done to provide a basis for a direct comparison of structural changes in the flow with no injection and the various streamwise locations in the injected flow. Had the structure been normalized with the local values of shear velocity and kinematic viscosity, the higher viscosity of the pressure solution and the lower wall shear stress resulting from the drag reduction would have had the following effects. The location of the peak values of $\overline{uv}$, v' and the production would have moved to lower values of y^+ and the peak values would have increased. In this way the structure of the drag-reduced flow would have appeared more like a Newtonian flow. The behaviour of u', however, would have still deviated significantly from that for a Newtonian flow. Normalization with the local value of shear velocity would have increased the peak in u' even further. Thus the transfer of energy from u' to v' would still appear to be inhibited. Therefore, normalizing on local

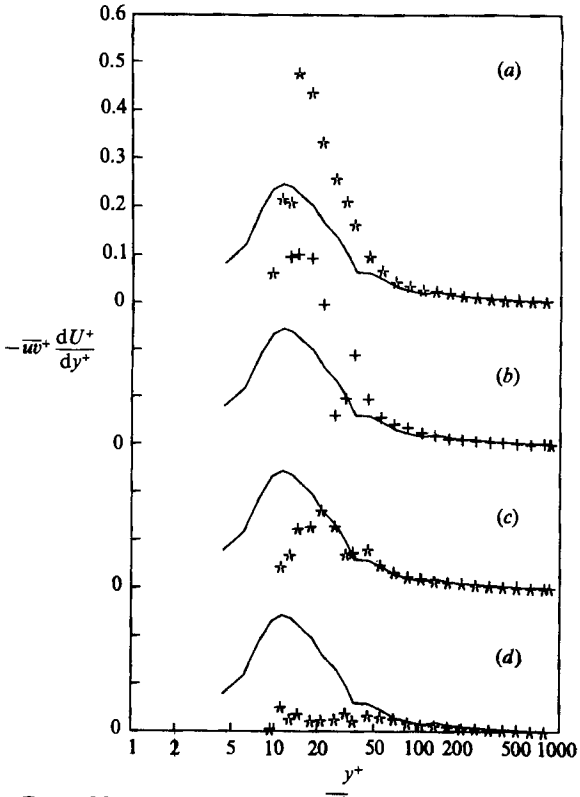

FIGURE 18. Reynolds stress production ($\overline{u^2}$ component) for flow with polymer injection: (*a*) $x = 25$ mm, (*b*) 50 mm, (*c*) 100 mm, (*d*) 200 mm; ——, fully developed flow.

values of shear velocity and kinematic viscosity would cause the turbulent structure to appear more like a Newtonian flow, but the conclusions drawn would not be affected.

Figure 20(*a*) shows the joint probability density function of uv as a function of u and v for the y-location corresponding to the peak in $\overline{uv}$ in the water flow with no injection ($y^+ = 45$). As expected, uv-realizations in quadrants II and IV ($u < 0, v > 0$ and $u > 0, v < 0$, respectively) are more probable than in quadrants I and III ($u > 0, v > 0$ and $u < 0, v < 0$), yielding a negative value for $\overline{uv}$.

Figures 20(*b*) and 20(*c*) show similar plots for $x = 100$ mm and 200 mm in the flow with polymer injection. These results are for the same y-locations as those shown in figure 20(*a*), but have reduced levels of $-\overline{uv}$ (see figure 16). In figure 20(*b*), the magnitude of the u-fluctuations has increased while v-fluctuation levels have decreased. There is also an increased probability of occurrence for uv-realizations in quadrants I and III. In figure 20(*c*) this behaviour is more pronounced, with the probability density function being nearly symmetric about the u-axis. At these locations, the principal axes for the Reynolds stress tensors have rotated toward the laboratory axes. This results in a reduced magnitude for $\overline{uv}$ and is responsible for the reduction in R_{uv} seen in figure 17.

The changes in the joint probability density functions caused by the polymer appear to be very subtle, even though the effect of these changes is to reduce $-\overline{uv}$ by more than 60% at $x = 200$ mm when compared to the water flow with no injection. To better determine the effect of these small changes, we can examine the

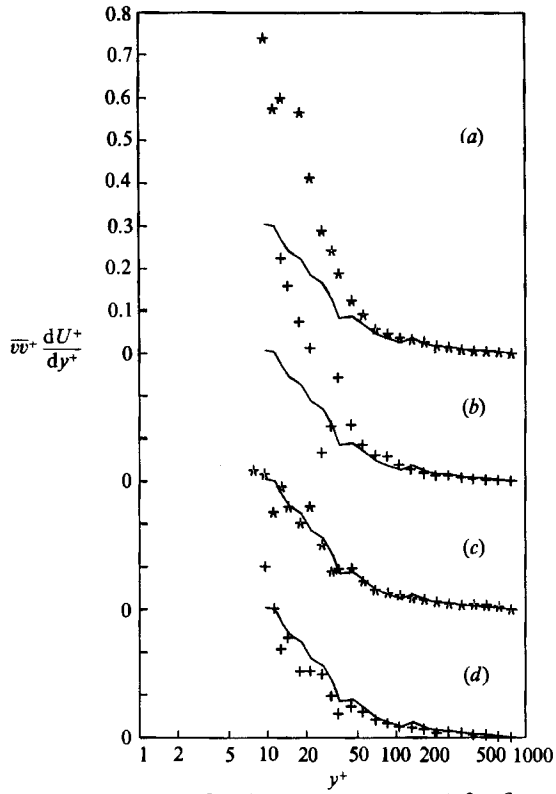

FIGURE 19. Reynolds stress production ($\overline{uv}$ component) for flow with polymer injection: (*a*) $x = 25$ mm, (*b*) 50 mm, (*c*) 100 mm, (*d*) 200 mm; ——, fully developed flow.

probability density function for uv weighted with the product $-uv$. This function, when integrated over the (u, v)-plane, gives the value of $-\overline{uv}$. By examining its behaviour, one can determine directly the contribution to $-\overline{uv}$ made by each location in the (u, v)-plane.

Figure 21(*a*) shows the relative contribution to $-\overline{uv}$ as a function of u and v for the water flow with no injection at the y-location corresponding to the $-\overline{uv}$ peak. This figure corresponds to the probability density function shown in figure 20(*a*). It can be seen that the largest contributions to $-\overline{uv}$ come from quadrants II and IV with relatively small negative contributions from quadrants I and III. The maximum positive and negative contributions are from u, v values that are removed from the u, v origin but are not at the extreme outer edges of the probability density function shown in figure 20(*a*). This is because, while realizations far removed from the origin result in large instantaneous uv values, the probability of occurrence is low and realizations near the origin, while more probable, have low uv-values.

Figure 21(*b*) shows similar results for $x = 100$ mm in the flow with polymer injection. These results are for the same y-location as figure 21(*a*) and correspond to the probability density function of figure 20(*b*). The differences caused by the polymer solution are clearly evident here. In quadrants II and IV, the maximum contributions are from smaller values of v and larger values of u than for the flow with no injection. In addition, the total contributions from these quadrants have been reduced owing to the decrease in the fluctuation level of v. In quadrants I and III, the reduction in v-fluctuations is more than offset by the increase in the u-

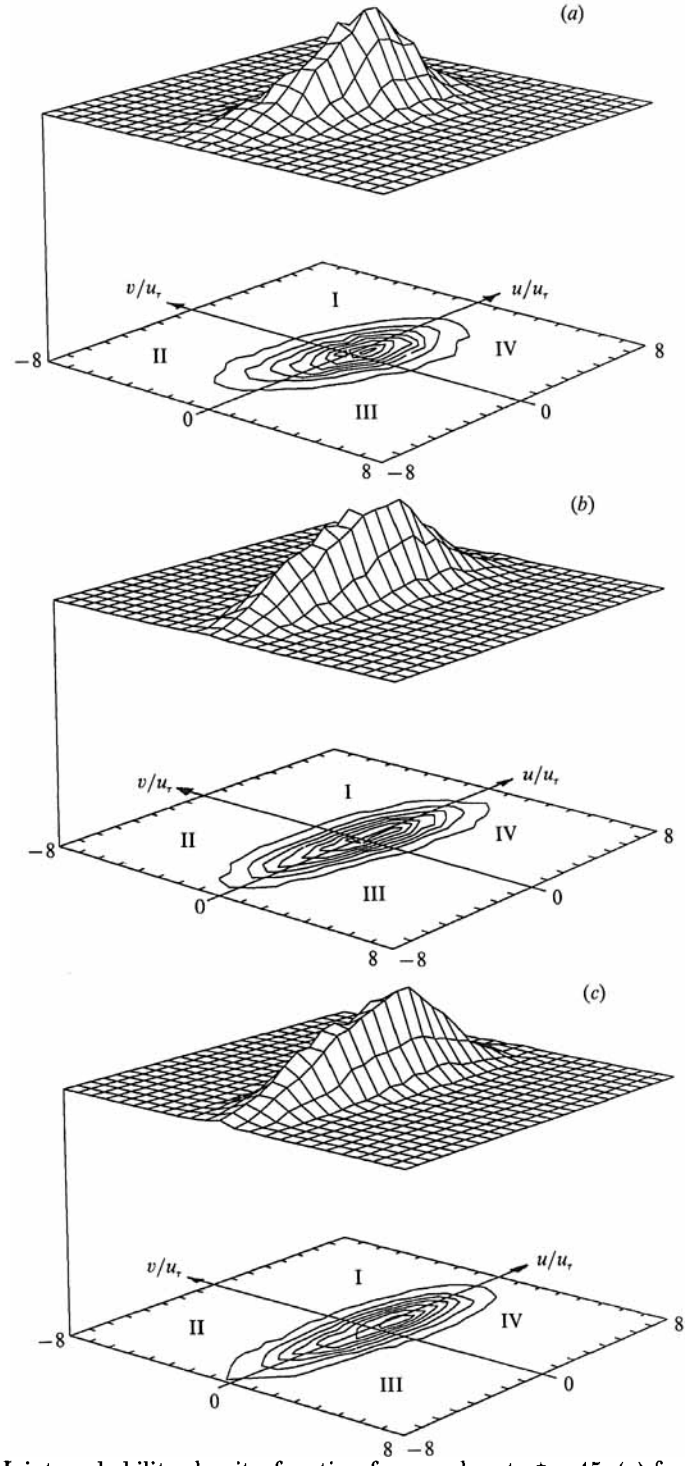

FIGURE 20. Joint probability density function for u and v at $y^+ = 45$, (*a*) for fully developed flow; and flow with polymer injection at (*b*) $x = 100$ mm and (*c*) $x = 200$ mm.

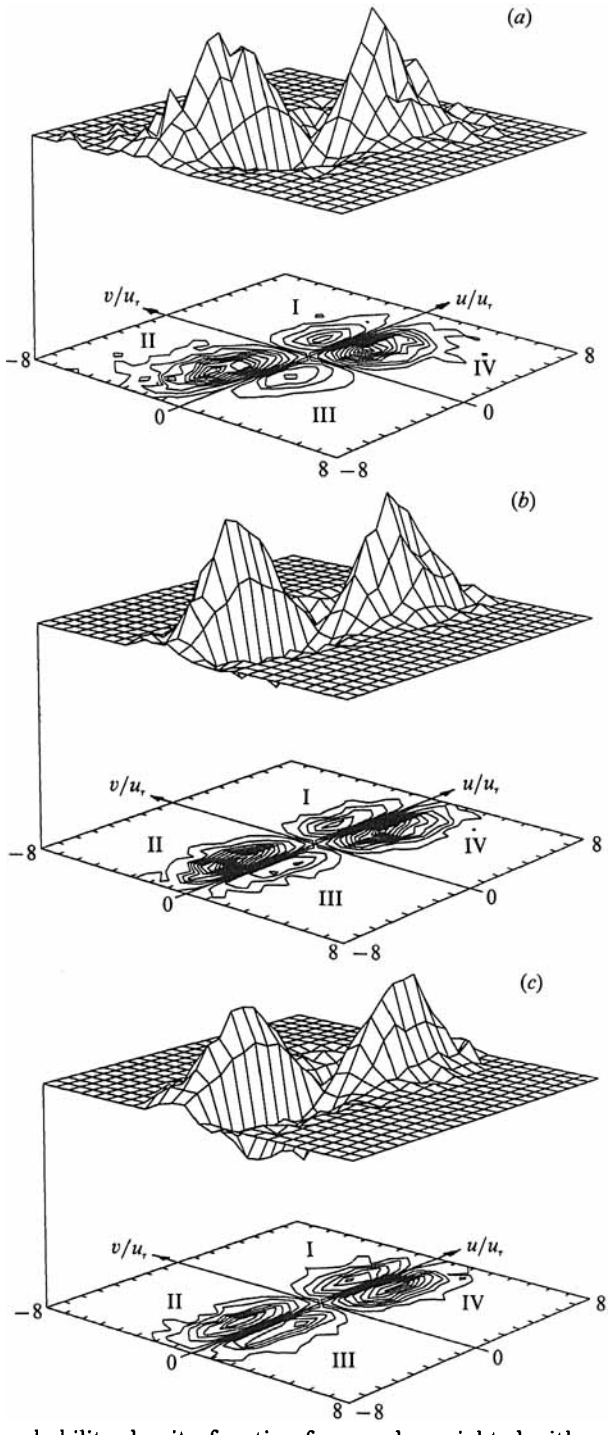

FIGURE 21. Joint probability density function for u and v weighted with $-uv$ at $y^+ = 45$, (a) for fully developed flow; and flow with polymer injection at (b) $x = 100$ mm and (c) $x = 200$ mm.

fluctuations. This results in a larger negative contribution to $-\overline{uv}$ from these quadrants than in the water flow. The decreased positive contribution from quadrants II and IV and the increased negative contribution from quadrants I and III result in a net decrease in the magnitude of $-\overline{uv}$.

Figure 21(*c*) show similar behaviour at $x = 200$ mm, except that the negative contributions to $-\overline{uv}$ from quadrants I and III have increased. These contributions offset more of the positive contributions from quadrants II and IV. This results in a further reduction in $-\overline{uv}$.

If one examines the location in the (u, v)-plane of the maximum positive and negative contributions to $-\overline{uv}$, one can gain an indication of what type of motions contribute to net turbulent momentum transport and how these are altered by the presence of the polymer solution. For the water flow (figure 21*a*) the largest positive contributions to $-\overline{uv}$ come from velocity fluctuations with a magnitude, $(u^2+v^2)^{\frac{1}{2}}$, of about $2.7u_\tau$ in quadrant II and $4.5u_\tau$ in quadrant IV. The largest negative contributions are from velocity fluctuations of about $2.2u_\tau$ in quadrants I and III. At $x = 100$ mm in the flow with polymer injection, the maximum positive contribution results from fluctuations of magnitude $3.3u_\tau$ in quadrant II and $4.6u_\tau$ in quadrant IV. The largest negative contributions are again from fluctuations of about $2.7u_\tau$ in both quadrants I and III. For $x = 200$ mm, the magnitude of the fluctuations resulting in the maximum positive contributions to $-\overline{uv}$ are essentially unchanged from those at $x = 100$ mm. However, the maximum negative contributions at $x = 200$ mm are from fluctuations with magnitude larger than $3u_\tau$.

These results show that velocity fluctuations which make the largest contributions, either positive or negative, to $-\overline{uv}$ increase in magnitude when the polymer solution is present. Taken together with the observed decrease in $-\overline{uv}$ which occurs, this confirms the finding of Luchik & Tiederman (1987) that the velocity scales associated with momentum transport are increased by the polymer solution.

4. Summary and conclusions

By examining a fully developed turbulent channel flow with polymer injection at the wall, this study attempted to gain new understanding of the way in which long-chain, high-molecular-weight, water-soluble polymers cause viscous drag reduction in turbulent wall flows. Two-component laser velocimeter measurements were made in a flow with polymer injection and a flow with water injection to examine the effect of both the injection process and the evolving polymer concentration field on the structure of turbulence.

The water flow results were consistent with those in the literature for fully developed, two-dimensional turbulent channel flow. However, a method was presented which uses two-component velocity measurements to determine the local wall shear velocity with higher accuracy ($\pm 3\%$) than can be obtained from pressure-drop measurements in channels with aspect ratios of 10 to 1 or less.

In the flow with polymer injection, the r.m.s. streamwise velocity levels were increased by about 15% at all streamwise locations. Initially, the injection process causes elevated levels of the r.m.s. of the wall-normal velocity and the turbulent shear stress. However, the action of the polymer solution subsequently reduced these quantities significantly below the levels present in the water flow for $x > 50$ mm. The decreased magnitude of $-\overline{uv}$ results from both the decrease in v' and a decrease in the degree of correlation between the u- and v-velocity fluctuations.

The polymer solution reduced the production rate for $\overline{u^2}$ while the production of

$\overline{uv}$ was not changed. The reduced levels of v' and $\overline{uv}$ along with the increase in u' caused by the polymer indicates that the polymer may alter the processes represented by the pressure–strain correlations. These correlations represent both the transfer of energy from $\overline{u^2}$ to $\overline{v^2}$ and the principal source of $\overline{uv}$ destruction. Assuming that the Reynolds stress transport equations are not significantly altered for the polymer solution, it is concluded that the polymer solution inhibits the redistribution from u' to v' and causes increased destruction of $\overline{uv}$.

Detailed examination of the u- and v-velocity fluctuations showed that the decrease in $-\overline{uv}$ caused by the polymer solution resulted from both a decrease in the positive contributions from quadrants II and IV and an increase in the negative contributions to $-\overline{uv}$ from quadrants I and III. It was also determined that although $-\overline{uv}$ was decreased by the polymer solution, the magnitude of the velocity fluctuations that most contributed to $-\overline{uv}$ increased.

This work was supported by the Office of Naval Research under contract number N000-14-83K-0183, NR 4322-754. A significant portion of the equipment used in this study was acquired under Office of Naval Research Grant N00014-87G-0040 with cost sharing by Purdue University, School of Mechanical Engineering. This support is gratefully acknowledged.

REFERENCES

Argumedo, A., Tung, T. T. & Chang, K. I. 1978 Rheological property measurements of drag-reducing polyacrylamide solutions. *J. Rheol.* **22**, 449.

Berman, N. S. 1989 Polymer contributions to transport equations. In *Drag Reduction in Fluid Flows: Techniques for Friction Control* (ed. R. J. H. Sellin and R. T. Moses), p. 21. Ellis Horwood.

Berner, C. & Scrivener, O. 1980 Drag reduction and turbulence in dilute polymer solutions. In *Viscous Flow Drag Reduction* (ed. G. R. Hough), p. 290. AIAA.

Bewersdorff, H. W. 1984 Effect of a centrally injected polymer thread on turbulent properties in pipe flows. In *Drag Reduction* (ed. R. J. H. Sellin and R. T. Moses), p. B4. University of Bristol.

Bradshaw, P. 1978 *Turbulence*. Topics in Applied Physics, Vol. 12, p. 25. Springer.

Cho, Y. I., Hartnett, J. P. & Park, Y. S. 1983 Solvent effects on the rheology of aqueous polyacrylamide solutions. *Chem. Engng Commun.* **21**, 369.

Edwards, R. V. 1987 Report of the special panel on statistical bias problems in laser anemometry. *Trans. ASME* I: *J. Fluids Engng* **109**, 89.

Finnicum, D. S. & Hanratty, T. J. 1985 Turbulent normal-velocity fluctuations close to a wall. *Phys. Fluids* **28**, 1654.

Gould, R. D., Stevenson, W. H. & Thompson, H. D. 1989 A parametric study of statistical bias in laser Doppler velocimetry. *AIAA J.* **27**, 1140.

Hoyt, J. W. 1984 Some highlights in the field of polymer drag reduction. In *Drag Reduction* (ed. R. J. H. Sellin & R. T. Moses), p. I.1-1. University of Bristol.

Hussain, A. K. M. F. & Reynolds, W. C. 1975 Measurements in fully developed turbulent channel flow. *Trans. ASME* I: *J. Fluids Engng* **97**, 568.

Karpuk, M. E. & Tiederman, W. G. 1976 Effect of finite-size probe volume upon laser-Doppler anemometry measurements. *AIAA J.* **14**, 1099.

Kim, J., Moin, P. & Moser, R. 1987 Turbulence statistics in fully developed channel flow at low Reynolds number. *J. Fluid Mech.* **177**, 133.

Kreplin, H. & Eckelmann, H. 1979 Behaviour of the three fluctuating velocity components in the wall region of a turbulent channel flow. *Phys. Fluids* **22**, 1233.

Ligrani, P. M. & Bradshaw, P. 1987 Spatial resolution and measurement of turbulence in the viscous sublayer. *Exps Fluids* **5**, 407.

LOGAN, S. E. 1972 Laser velocimeter measurements of Reynolds stress and turbulence in dilute polymer solutions. *AIAA J.* **7**, 962.

LUCHIK, T. S. & TIEDERMAN, W. G. 1986 Effect of spanwise probe volume length on laser velocimeter measurements in wall bounded turbulent flows. *Exps Fluids*, **3**, 339.

LUCHIK, T. S. & TIEDERMAN, W. G. 1987 Timescale and structure of ejections and bursts in turbulent channel flows. *J. Fluid Mech.* **174**, 529.

LUCHIK, T. S. & TIEDERMAN, W. G. 1988 Turbulent structure in low concentration drag-reducing channel flows. *J. Fluid Mech.* **190**, 241.

MANSOUR, N. N., KIM, J. & MOIN, P. 1988 Reynolds-stress and dissipation-rate budgets in a turbulent channel flow. *J. Fluid Mech.* **194**, 15.

MCCOMB, W. D. & RABIE, L. H. 1982 Local drag reduction due to injection of polymer solutions into turbulent flow in a pipe. Part I: Dependence on local polymer concentration; Part II: Laser-Doppler measurements of turbulent structure. *AICHE J.* **28**, 547.

MCLAUGHLIN, D. K. & TIEDERMAN, W. G. 1973 Biasing correction for individual realization of laser velocimeter measurements in turbulent flows. *Phys. Fluids* **16**, 2082.

METZNER, A. B. & ASTARITA, G. 1967 External flows of viscoelstic materials: Fluid property restrictions on the use of velocity-sensitive probes. *AIChE J.* **13**, 550.

MOIN, P. & KIM, J. 1982 Numerical investigation of turbulent channel flow. *J. Fluid Mech.* **118**, 341.

MOSER, R. D. & MOIN, P. 1987 The effects of curvature in wall bounded turbulent flows. *J. Fluid Mech.* **175**, 479.

MYSELS, K. 1949 Flow of thickened fluids. US Patent No. 2492173.

NAGANO, Y. & HISHIDA, M. 1985 Production and dissipation of turbulent velocity and temperature fluctuations in fully developed pipe flow. In *Proc. Fifth Intl Symp. on Turbulent Shear Flows, Cornell University*, p. 14.19.

REISCHMAN, M. M. & TIEDERMAN, W. G. 1975 Laser Doppler anemometer measurements in drag-reducing channel flows. *J. Fluid Mech.* **70**, 369.

RUDD, M. J. 1972 Velocity measurements made with the laser Dopplermeter in turbulent pipe flow of a dilute polymer solution. *J. Fluid Mech.* **51**, 673.

RYSKIN, G. 1987 Calculation of the effects of a polymer additive on converging flow. *J. Fluid Mech.* **178**, 423.

SPALART, P. 1988 Direct simulation of a turbulent boundary layer up to $R_\theta = 1410$. *J. Fluid Mech.* **187**, 61.

TIEDERMAN, W. G., LUCHIK, T. S. & BOGARD, D. G. 1985 Wall layer structure and drag reduction. *J. Fluid Mech.* **156**, 419.

TOMS, B. A. 1949 Observations on the flow of linear polymer solutions through straight tubes at large Reynolds numbers. In *Proc. Intl Rheological Congress, Holland, 1948*, Vol. II, pp. 135–141. North-Holland.

TSAI, C. F. & DARBY, R. 1978 Nonlinear viscoelastic properties of very dilute drag-reducing polymer solutions. *J. Rheol.* **22**, 219.

WALKER, D. T. & TIEDERMAN, W. G. 1987 Near-field effects of polymer wall injection on turbulent channel flow. In *Proc. Twentieth Midwest Mechanics Conference*, Vol. 14a (ed. W. Sodel & J. F. Hamilton), p. 76. Purdue University.

WALKER, D. T. & TIEDERMAN, W. G. 1989 The concentration field in a turbulent channel flow with polymer injection at the wall. *Exp. Fluids* **8**, 86.

WALKER, D. T., TIEDERMAN, W. G. & LUCHIK, T. S. 1986 Optimization of the injection process for drag reducing additives. *Exps Fluids* **4**, 114.

WEI, T. & WILLMARTH, W. W. 1989 Reynolds-number effects on the structure of a turbulent channel flow. *J. Fluid Mech.* **204**, 57.

WILLMARTH, W. W., WEI, T. & LEE, C. O. 1987 Laser anemometer measurements of Reynolds stress in a turbulent channel flow with drag reducing polymer additives. *Phys. Fluids* **30**, 933.